Spectral, energy, and angular characteristics of supercontinuum formed by a femtosecond-duration pulsed laser radiation in air

A.A. Zemlyanov and Yu.E. Geints

Institute of Atmospheric Optics,
Siberian Branch of the Russian Academy of Sciences, Tomsk

We have studied, using a numerical method, transformation of the spectral, energy, and angular characteristics of the supercontinuum formed by a femtosecond-duration pulsed laser radiation in air. It has been shown that transformation of the frequency spectrum of an ultrashort pulse after its self-focusing and the fraction of its energy transformed into the energy of supercontinuum are mainly determined by the length of a light filament. It has been established that the angular size of a femtosecond-duration pulsed laser radiation beam sharply increases after passing through the region of a global nonlinear focus and then it gradually grows in the zone of beam filamentation approaching some limiting value. The increase of the initial power of radiation yields an increase of the limiting angular divergence of the beam. The angular size of the spectral components of supercontinuum in its IR and visible wings is larger than the beam divergence averaged over the entire spectrum. The excess divergence is larger in the IR wing and can reach two times over the average one.

Introduction

At present, the problems on propagation of high-power ultrashort emission through the atmosphere and the prospects of using nonlinear interaction effects for diagnostics of some atmospheric characteristics are being actively discussed in the literature.[1–5] High peak power of femtosecond pulses determines their propagation through the atmosphere in the mode of self-channeling and strong spatiotemporal phase self-modulation. As a result of the dynamic balance between the focusing effect due to Kerr nonlinearity and defocusing effect of plasma, generated at multiphoton ionization of the medium in the radiation channel, the beam filamentation and enrichment of the radiation frequency spectrum with the formation of supercontinuum take place. The spectral width of this radiation is rather large. Thus, for the initial radiation with a central wavelength of $\lambda_0 = 800$ nm the supercontinuum spectrum has captured the ultraviolet and near infrared spectral ranges.[2,6] With the use of such broadband source it has become possible to detect simultaneously, at many frequencies, gas and aerosol atmospheric components and atmospheric pollutants.[3,4]

The physical pattern of filamentation and the formation of supercontinuum radiation in the atmosphere was discussed in many papers, both experimental and theoretical (the overview of these papers can be found in the literature[1,3]). In the experimental investigations, only averaged over space and time characteristics are being studied such as energy of laser beams, the pulse energy in the entire spectral range and its different parts, the transverse distribution of energy density in different spectral ranges, the filament length, and the number of filaments. The subjects of the experimental investigations determine the field of theoretical studies. Such theoretical models become demandable, which were productive when interpreting the experimental data and realized the forecast of propagation of high-power femtosecond radiation at the distance comparable with the diffraction length of a beam.

In this paper we use, to study the propagation of high-power femtosecond pulses in the air, the methodology of effective (integral) laser radiation parameters developed in Ref. 7, such as pulse energy, effective beam radius, spectral pulse width, global and spectral angular divergence. We have established the relations between the effective characteristics of ultrashort radiation at each point of the path and the initial values of power, beam radius, as well as with the length of light filament induced in the medium by laser radiation.

Method of investigation. Basic approximations

The paper describes the computer simulation of self-action of ultrashort light pulse in the atmosphere on a horizontal path without the presence of aerosols and turbulence. Nonlinear Schrödinger equation (NSE) was solved numerically for a slowly varying complex amplitude of the electromagnetic radiation

field $U(\mathbf{r}_\perp, z, t)$ with the account of the air frequency dispersion of the second order, instantaneous and inertial components of the Kerr effect, nonlinear absorption and refraction of radiation by plasma formed due to multiphoton gas ionization. This equation has the following form (see, for example, Refs. 1 and 7):

$$\left\{\frac{\partial}{\partial z} - \frac{i}{2n_0 k_0}\nabla_\perp^2 + i\frac{k_\omega''}{2}\frac{\partial^2}{\partial t^2}\right\}U(\mathbf{r}_\perp, z; t) -$$

$$- ik_0 n_2\left\{(1 - \mu)|U|^2 + \mu\int\limits_{-\infty}^{\infty}\mathrm{d}t'\Lambda(t - t')\left|U(t')\right|^2\right\}U(\mathbf{r}_\perp, z; t) +$$

$$+ \frac{\eta_{\mathrm{cas}}}{2}(1 + i\omega_0\tau_{\mathrm{c}})\rho_{\mathrm{e}}(\mathbf{r}_\perp, z; t)U(\mathbf{r}_\perp, z; t) +$$

$$+ \frac{\eta_{\mathrm{MPA}}^{(m)}}{2}|U|^{2m-2}U(\mathbf{r}_\perp, z; t) = 0,$$

where $|\mathbf{r}_\perp| = \sqrt{x^2 + y^2}$; $k_0 = n_0\omega_0/c$ is the wave number, ω_0 is the central frequency of laser radiation; c is the speed of light in vacuum; $k_\omega'' = \partial k/\partial\omega^2 = 0.21$ fs^2/cm is the dispersion of the light pulse group velocity in the air (at the wavelength $\lambda_0 = 800$ nm); $n_2 = 3.2\cdot10^{-19}$ cm^2/W is the coefficient at the nonlinear term of the gas index of refraction n_0, μ is the specific part of the Kerr inertial effect with the response function $\Lambda(t - t')$ in the sum variation of the nonlinear index of refraction (usually it is taken to be equal 0.5), $\tau_{\mathrm{c}} = 350$ fs is the characteristics time of an electron collision, $\eta_{\mathrm{MPA}}^{(m)}$ is the m-photon ionization rate, η_{cas} is the cross section of the molecular cascade ionization. As $\Lambda(t - t')$ we use a simplified expression following from the model of a damped oscillator: $\Lambda(t) = \theta(t)\Omega\exp(-t/\tau_{\mathrm{d}})$, where $\Omega \simeq 20$ THz is the frequency of oscillations, $\tau_{\mathrm{d}} \simeq 70$ ns is the characteristic attenuation, $\theta(t)$ is the Heaviside step function.

The variation in time of the free electron concentration ρ_{e} was calculated using the model of quasiequilibrium plasma without the account of recombination losses:

$$\frac{\partial\rho_{\mathrm{e}}}{\partial t} = \frac{\eta_{\mathrm{MPA}}^{(m)}}{m\hbar\omega_0}|U|^{2m} + \frac{\eta_{\mathrm{cas}}}{n_0\Delta E_i}\rho_{\mathrm{e}}|U|^2,$$

where $\Delta E_i = 12.1$ eV is the ionization potential of the oxygen atom. Eight quanta ($m = 8$) at $\lambda_0 = 800$ nm are needed to ionize O_2 atom, in this case, the ionization coefficient $\eta_{\mathrm{MPA}}^{(m)}$ was determined from analysis of experimental data[8] as $\eta_{\mathrm{MPA}}^{(m)} = 3.6\cdot10^{-121}$ m$^{13}\cdot$W^{-7}. The cross section of the cascade ionization was taken to be equal to $\eta_{\mathrm{cas}} = 5.1\cdot10^{-22}$ m^2.

The procedure of the numerical integration of the nonlinear Schrödinger equation was performed with the use of the method of separation at each step along the evolution variable z of the initial problem into two subtasks: nonlinear subtask when the formation of a nonlinear field phase is calculated, and a linear one, when free diffraction and the dispersion of a wave packet with the phase front determined at the preceding step result in the transformation of the field amplitude. To increase the stability of the calculation, a combination of the Fourier spectral method (in time) was used together with an implicit three-layer difference scheme of the Crank–Nicholson scheme type (transverse coordinates) and adaptive correction of a grid step along the evolution variable. The efficient radiation parameters were calculated as the integral moments of the second order from local field characteristics using the formulae from Ref. 7, and also presented below in this paper.

In the numerical experiments an ideal femtosecond laser pulse with a Gaussian profile in time and space was set

$$U(\mathbf{r}_\perp, z = 0; t) = U_0\exp\left\{-\frac{\mathbf{r}_\perp^2}{2R_0^2}\left(1 + \frac{ik_0 R_0^2}{F}\right)\right\}\exp\left\{-\frac{t^2}{2t_{\mathrm{p}}^2}\right\}$$

with the following initial parameters the wavelength $\lambda_0 = 800$ nm, the duration (at the level e^{-1} of the intensity maximum) $t_{\mathrm{p}} = 80$ fs, the radius $R_0 = 1$ mm. The initial radius of the radiation phase front curvature F was chosen to be equal to a doubled Rayleigh length $L_{\mathrm{R}} = k_0 R_0^2/2$ so that $F = 2L_{\mathrm{R}}$. The radiation self-focusing with such symmetric profile results in the formation of one waveguide channel (light filament) on the beam axis. Further we shall use the normalized variables: $r_\perp/R_0$, z/L_{R}, F/L_{R}, t/t_{p}.

Effective spectral width of supercontinuum radiation

The parameter characteristic of effective spectral width $\Delta\omega$ of a femtosecond-duration radiation pulse in the atmosphere is central moment of the second order of the pulse spectral density $\left|F_\omega(r_\perp, z, \omega)\right|^2$ averaged over the beam cross section

$$\Delta_\omega(z) = \left[\frac{1}{E(z)}\iint\limits_{-\infty}^{\infty}\mathrm{d}^2\mathbf{r}_\perp\int\limits_{-\infty}^{\infty}\mathrm{d}\omega\left|F_\omega(\mathbf{r}_\perp, z; \omega)\right|^2(\omega - \omega_{\mathrm{gr}})^2\right]^{1/2}, \quad (1)$$

where $F_\omega(\mathbf{r}_\perp, z; \omega)$ is the Fourier transform of the light field complex amplitude $U(\mathbf{r}_\perp, z; t)$ in the space of time frequencies;

$$\omega_{\mathrm{gr}}(z) = [1/E(z)]\iint\limits_{-\infty}^{\infty}\mathrm{d}^2\mathbf{r}_\perp\int\limits_{-\infty}^{\infty}\mathrm{d}\omega\left|F_\omega(\mathbf{r}_\perp, z; \omega)\right|^2\omega$$

is the position of the center of gravity of the pulse frequency spectrum, and

$$E(z) = \iint_{-\infty}^{\infty} d^2\mathbf{r}_\perp \int_{-\infty}^{\infty} d\omega \left| F_\omega(\mathbf{r}_\perp, z; \omega) \right|^2$$

is its total energy. Within the framework of these definitions, real spectral contour of radiation at each point z of the path is replaced by a symmetric Gaussian profile with the center on the frequency axis at a point $\omega_{gr}(z)$ and the parameter of the contour width $\Delta_\omega(z)$.

Figure 1 shows the evolution, along the path, of the mean width of the frequency spectrum Δ_ω of a femtosecond laser pulse at its propagation in the air in the filamentation mode. Figure 1 also shows the beam radius R_{-1}, determined at the level e^{-1} of the maximum of transverse distribution of the light energy density $w(\mathbf{r}_\perp, z)$ at each point of the path. Curves in this figure were calculated at variation of the initial power of laser pulse P_0, set by the dimensionless parameter $\eta = P_0/P_c$, where P_c is the critical power of self-focusing in the air ($P_c = 3.2$ GW for radiation at the wavelength $\lambda = 800$ nm).
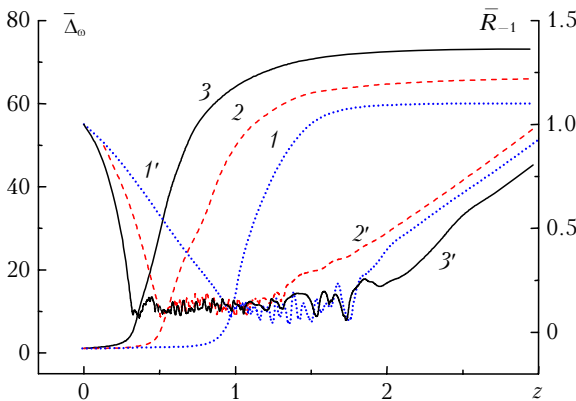

Fig. 1. Normalized mean width of the frequency range $\bar{\Delta}_\omega = \Delta_\omega(z)/\Delta_\omega(0)$ (*1–3*) and the transverse beam radius $\bar{R}_{-1} = R_{-1}/R_0$ (*1'–3'*) at propagation in air of a femtosecond-duration radiation with the initial peak power $\eta = 2$ (*1*), 5 (*2*), and 10 (*3*).

One can notice from analysis of the dependences shown in Fig. 1 that at the initial part of the path when the transverse beam compression occurs due to Kerr effect, the radiation spectrum width remains practically invariable up to the moment of the filament formation. In this case, as follows from Fig. 2, where the dependence of the value ω_{gr} on the propagation distance is shown, the center of gravity of the spectral curve is shifted to the Stokes frequency range (negative values relative to the central radiation frequency ω_0). Such a shift of the spectrum is caused by the inertial component in the total Kerr nonlinearity of the medium, which is realized during ~70 fs (based on the data from Ref. 9), the time necessary for swinging the

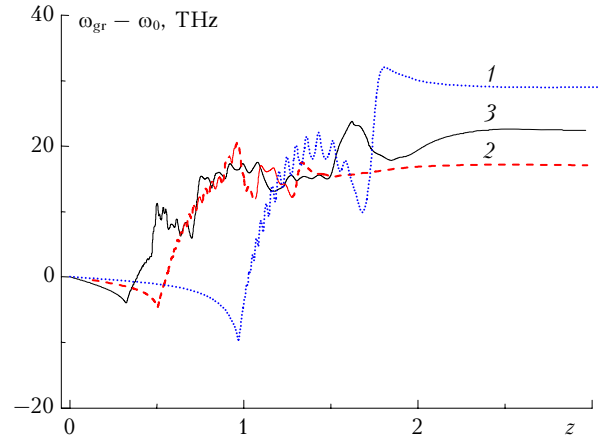vibration–rotation transitions of nitrogen and oxygen molecules.

Fig. 2. The frequency of center of gravity of the pulse spectrum ω_{gr} depending on the evolution variable for $\eta = 2$ (*1*), 5 (*2*), and 10 (*3*).

In order to understand the physical pattern of the behavior of the parameters Δ_ω and ω_{gr} along the path we consider the model of one-dimensional light wave propagation in the medium with nonlinearity of Kerr and plasma types. The frequency deviation of such a wave $\partial\omega(z, t)$ at the distance z is determined by the nonlinear component of the wave phase φ_N as follows[10]:

$$\delta\omega(z,t) = \partial\varphi_N(z,t)/\partial t \propto -k_0 z \frac{\partial}{\partial t}[\Delta n_K(z,t) + \Delta n_p(z,t)], \quad (2)$$

where Δn_K and Δn_p are the contributions to the variation of the index of refraction of the medium due to Kerr effect and plasma generation, respectively, given by the following formulae:

$$\Delta n_K(z,t) = \frac{8\pi n_2}{c n_0}\left[(1-\mu)I(z,t) + \mu\int_{-\infty}^{t} I(z,t')\Lambda(t-t')dt'\right], \quad (3)$$

$$\Delta n_p(z,t) = -\frac{\eta_{cas} l_c \rho_e(z,t)}{2}. \quad (4)$$

where I is the radiation intensity, l_c is the electron mean free path.

We consider that the increase of the free electron concentration in the beam channel is mainly determined by the process of multiphoton ionization, i.e.,

$$\rho_e(t) = \rho_0 \eta_{MPA}^{(m)} \int_{-\infty}^{t} I^m(t')dt',$$

where ρ_0 is the concentration of gas molecules.

Then, substituting Eqs. (3) and (4) in Eq. (2), we obtain:

$$\delta\omega(z,t) \propto -k_0 z\left[(1-\mu)A\frac{\partial I(z,t)}{\partial t} + \mu B I(z,t) - C I^m(z,t)\right], \quad (5)$$

where $A = 8\pi n_2/cn_0$ $B = A\,\Omega,$ $C = 1/2\eta_{cas}\,l_c N_0 \eta_{MPA}^{(m)}$ is the constants independent of time, N_0 is concentration of neutral gas molecules.

From Eq. (5) it follows that at the initial stage of the beam self-focusing the symmetric broadening of the pulse spectrum, described by the first term, is modified by a fixed-sign inertial Kerr nonlinearity; as a result, the radiation spectrum obtains a shift to the low frequency range. With the increase of the peak intensity near the nonlinear beam focus and the corresponding increase of the free electron concentration ρ_c in Eq. (5) the "plasma" component starts to prevail, which shifts the center of gravity of the spectrum to the UV range.

The light filament is characterized by the quasi-constant value of the peak radiation intensity I_f (in the air $I_f \sim 10^{14}$ W/cm^2 at $\lambda_0 = 800$ nm) and by the value of the cross size in the range $\sim 70-150$ μm, which are determined by the characteristics of the medium n_2 and $\eta_{MPA}^{(m)}$. Therefore, the spectral pulse broadening in the beam filamentation zone, following Eq. (5), is proportional to the effective length of the filament L_f:

$$\Delta_\omega(z = L_f) \sim k_0 L_f K(I_f),$$

where K is the coefficient given by an expression in square brackets in the right-hand side of Eq. (5). Such a growth of the parameter Δ_ω, close to a linear one at the stage of beam filamentation, is seen in Fig. 1 at all levels of the initial radiation power used in calculations.

After the destruction of a filament due to a sharp decrease of the intensity, the spectral radiation transformation is completed, and its spectral width, as follows from Fig. 1, is stabilized at a certain level $\Delta_{\omega\,max}$. The value of this level, as calculations show, is also proportional to the beam filamentation length L_f (see Fig. 3).
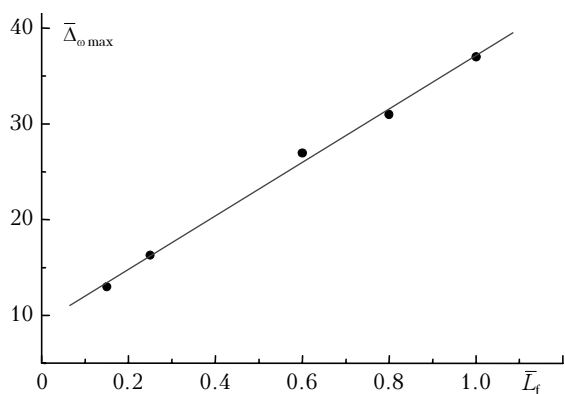

Fig. 3. The normalized mean width of the pulse frequency spectrum $\bar{\Delta}_\omega$ depending on the light filament length $\bar{L}_f = L_f/L_R$: the calculated data are denoted by dots and the linear regression is presented by solid line.

It should be noted that in the dependence $R_{-1}(z)$ presented in Fig. 1 the parameter L_f was determined

as the distance between the first and last minimum, i.e., at variation of the initial power of the radiation pulse P_0. It is worth noting that similar result is obtained in the case if the focal length of a beam is varied at a fixed P_0 level, because it is known that the filament length decreases with the increasing sharpness of focusing.[10] Hence, the dependence (5) is rather universal and it correctly presents the fact that the growth of the pulse spectral width takes place primarily in the beam filamentation zone, where its intensity peaks, and the value $\Delta_{\omega\,max}$ is proportional to the extension of this zone.

Energy of the supercontinuum

Knowledge of the laws of evolution of the effective values Δ_ω and ω_{gr} at laser pulse propagation through a medium makes it possible to calculate the part of light energy in the high-frequency and low-frequency spectral wings formed as a result of nonlinear phase self-modulation of the initial radiation, or, in other words, — the supercontinuum energy E_{SC}. Actually, using the Gaussian shape of an averaged pulse spectrum and defining the frequencies of supercontinuum in its "red" $\omega < \omega_{gr}$ and "blue" $\omega_+ > \omega_{gr}$ wings, we obtain the following expression for $E_{SC}(z)$:

$$E_{SC}(z) = 2T_e(z)E_0 \times$$

$$\times \left\{ 1 - \frac{1}{2}\left[\mathrm{erf}\left(\frac{\omega_+ - \omega_{gr}(z)}{\Delta_\omega(z)}\right) + \mathrm{erf}\left(\frac{-\omega_- + \omega_{gr}(z)}{\Delta_\omega(z)}\right) \right] \right\},$$

$$\omega \in (-\infty; \omega_-] \cup [\omega_+; \infty), \qquad (6)$$

where $T_e(z) = E(z)/E_0$ is the coefficient of the radiation power transmission, ω_+ and ω_- are the boundary frequencies of the supercontinuum, erf(x) is the error function.

The values of the normalized energy of supercontinuum $\bar{E}_{SC} = E_{SC}/E_0$ depending on the light filament length are shown in Fig. 4.
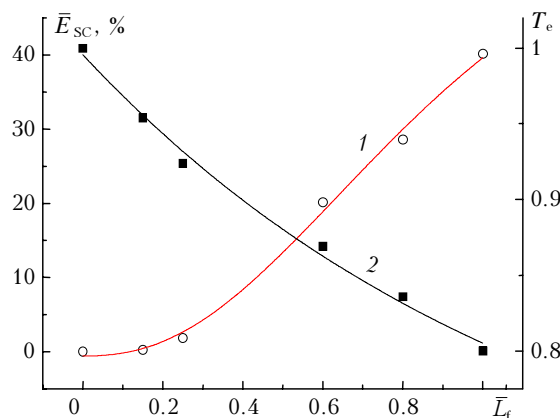

Fig. 4. Relative energy of supercontinuum $\bar{E}_{SC}$ (*1*) and the coefficient of beam energy transfer T_e (*2*) as functions of the normalized length of light filament L_f; the calculated data are denoted by dots; the spline-approximation is shown by solid lines.

In the calculations the boundary frequencies of supercontinuum ω_- and ω_+ were given by the values corresponding to the wavelengths of 850 and 750 nm, i.e., at the boundaries of the initial pulse spectrum and the values of T_e were calculated at the end of the path $z = 3$ for different initial pulse power. Figure 4 shows that with the increase of the light filament length the values of E_{SC} increase also. In the extended filaments ($\bar{L}_F > 0.4$) a considerable transformation of the initial radiation energy to the supercontinuum energy can take place. It is evident that, later on, the growth of the level of this transformation will be restricted by the increased losses of the radiation energy on the medium ionization.

Spectral angular divergence of the laser beam

In propagating of a high-power laser pulse through a medium in the regime of nonstationary self-focusing, transformations of its angular spectrum take place along with the variation of its spectral and energy characteristics. Consider now the spectral angular divergence of a laser beam $\theta_\omega(z)$, which we define by the effective width of the spatial spectrum of radiation of a corresponding spectral range:

$$\theta_\omega^2(z) = \frac{\lambda_0}{2\pi}\left[\frac{1}{E_\omega(z)}\iint\limits_{-\infty}^{\infty}d^2k_\perp \left|S_\omega(\mathbf{k}_\perp, z;\omega)\right|^2 \left|\left(\mathbf{k}_\perp - \mathbf{k}_g^\omega\right)\right|^2\right] . (7)$$

where

$$S_\omega = \int\limits^{\infty} dt S(\mathbf{k}_\perp, z, t)\exp(i\omega t),$$

$$S(\mathbf{k}_\perp, z, t) = \int d^2r_\perp \cdot U(\mathbf{r}_\perp, z, t)\exp(i\mathbf{k}_\perp \mathbf{r}_\perp)$$

denote the angular spectrum of radiation, $\mathbf{k}_\perp = (k_x, k_y)$ are the spatial frequencies,

$$E_\omega(z) = \iint\limits_{-\infty}^{\infty} d^2k_\perp \left|S_\omega(\mathbf{k}_\perp, z;\omega)\right|^2 = \iint\limits_{-\infty}^{\infty} d^2r_\perp \left|F_\omega(\mathbf{r}_\perp, z;\omega)\right|^2$$

is the spectral density of the radiation energy,

$$\mathbf{k}_g^\omega(z;\omega) = 1/E_\omega(z)\iint\limits_{-\infty}^{\infty} d^2k_\perp \left|S_\omega(\mathbf{k}_\perp, z;\omega)\right|^2 \mathbf{k}_\perp$$

is the angular shift of the beam axis, $E(z) = \int d\omega E(z)$ is the total energy of radiation. Equation (7) shows that due to the nonstationarity of the self-action process (the nonlinear variations of the medium refractive index induced by the light wave field have time scale comparable with the duration of a laser pulse) each spectral component of the light pulse at the frequency ω has its angular divergence $\theta_\omega(z)$.

Consider now in a more detail the angular behavior of the spectral components of supercontinuum radiation formed at filamentation of a femtosecond light beam. Let us separate out the effect of the so-called conical emission (CE) of radiation in the anti-Stokes spectral range accompanying the filament in the air. The conical emission was observed visually in the form of concentric rings relative to the axis of a beam, colored in red to green.[14-17] Qualitative and quantitative explanation of this effect was presented most completely in Ref. 13 based on the mechanism of the phase self-modulation of radiation in plasma formed in the leading edge of a pulse. In the optically dense media, such as fused silica, Ref. 15, or water, Ref. 16, frequency dispersion of the medium is considered as the basic effect that causes the conical emission of a femtosecond radiation, which determines the angular position of rings depending on the wavelength of a spectral component of the supercontinuum radiation.

Figure 5 shows, for example, a typical 2D intensity distribution over spatial $|\mathbf{k}_\perp|/k_0$ and time ω frequencies of a femtosecond pulse $\left|S_\omega(\mathbf{k}_\perp;\omega)\right|^2$ propagating in the air.
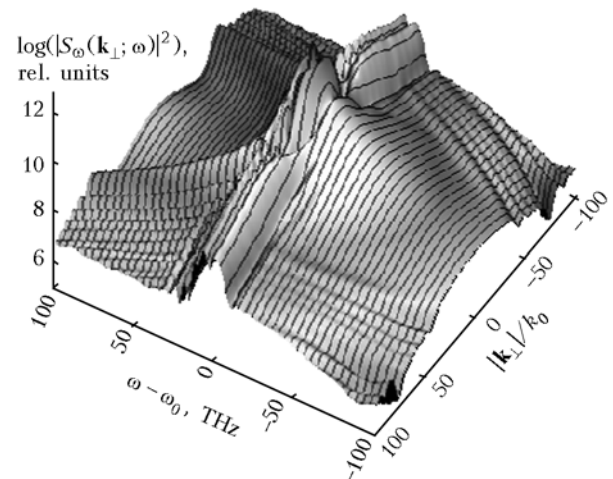

Fig. 5. The distribution of spectral intensity of a femtosecond pulse over the spatial and temporal frequencies at $\eta = 5$ and $z = 1.1$.

The distribution shown corresponds to a point of the path where the filament exists. The different shape of surfaces $\left|S_\omega(\mathbf{k}_\perp;\omega)\right|^2$ in the Stokes and anti-Stokes spectral ranges is shown clearly in the figure.

In the "blue" wing, formed by the plasma nonlinearity of the medium, we observe linear dependence of the angular coordinate of the maximum of spectral intensity on frequency that is characteristic of conical emission. At the same time the angular position of maximum of the function $\left|S_\omega(\mathbf{k}_\perp;\omega)\right|^2$ for frequencies with "red" shift relative to ω_0 corresponds to the near-axis propagation of Stokes radiation.

However, in spite of the above distinctions, the behavior of the spectral angular divergence of radiation $\theta_\omega(z)$, determined by the expression (7) in both spectral ranges, as follows from Fig. 6, is found to be similar.
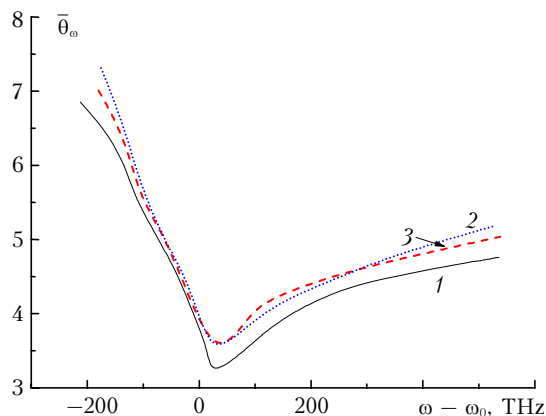

Fig. 6. Spectral dependence of normalized angular divergence of supercontinuum radiation $\bar{\theta}_\omega = \theta_\omega / \theta_D$ at filamentation of a femtosecond pulse ($\eta = 5$) in air at different distance $z = 1.2$ (*1*); 1.5 (*2*); 2.0 (*3*). θ_D is beam divergence due to diffraction.

The described dependences have *V*-shapes with minimum close to the central frequency of a wave packet and more flat slope of the "blue" wing due to the effect of plasma nonlinearity.

It should be emphasized once more that spectral components with the same $|\omega - \omega_0|$ value have close angular divergence but the intensities of these components are localized in space in different way: the anti-Stokes component propagates in the form of a concentric ring with peak intensity at $|\mathbf{k}_\perp| / k_0 = \theta_0(\omega)$, while the Stokes component of supercontinuum, due to a self-induced Kerr lens, form a circle with maximum on the beam axis. For this reason in the experiments the conical emission in the infrared wing of the femtosecond radiation spectrum, propagating in the air, is not recorded, Ref. 12.

Figure 6 shows one more characteristic of the conical emission, first detected in Ref. 12, namely, weak dependence of the angular position of rings along the filament. Thus, in the plots presented this variation makes less than 10% in moving from the beginning to the end of the filamentation region that points to the relative stability of energy and dimension parameters of the filament.

Global angular divergence of a femtosecond-duration laser beam

The behavior of divergence as a whole (global angular divergence) $\theta(z)$ is described by the relation obtained by averaging over the spectral radiation energy $E_\omega(z)$ of Eq. (7). Thus for a square of the parameter $\theta(z)$ we have

$$\theta^2(z) = \left[\int_{-\infty}^{\infty} E_\omega(z)\mathrm{d}\omega \right]^{-1} \int_{-\infty}^{\infty} E_\omega(z)\theta_\omega^2(z;\omega)\mathrm{d}\omega . \quad (8)$$

In the theory of the stationary radiation self-focusing[17] the angular beam divergence is constant up to its nonlinear focus and is equal to the value

$$\theta^2(z) = \theta_D^2 + \frac{4\pi n_2}{P_0 c n_0}\left[\int\int_{-\infty}^{\infty}\mathrm{d}^2 r_\perp \mathbf{r}_\perp \left(\nabla I^2(\mathbf{r}_\perp, z = 0) - \nabla I^2(\mathbf{r}_\perp, z) \right) \right],$$

where

$$\theta_D = 1/kR_0\sqrt{(1 + 4L_R^2/F^2)}$$

is the angular beam divergence due to its diffraction in the linear medium, I is the radiation intensity.

Figure 7 shows (curve *1*) the global angular beam divergence $\theta(z)$ as a function of the evolution variable at the radiation filamentation in the air. The Kerr self-focusing of radiation is accompanied by a sharp increase of energy density on the beam axis and avalanche-type increase of the free-electron concentration at the medium photoionization followed by the plasma formation (curve *3*). The light filament is formed in a nonlinear beam focus (the point z_1 on the curve *3* in Fig. 7), and here the angular divergence reaches its local maximum. The level of peak electron density $\rho_e = 10^{21}$ m^{-3} was chosen as the filamentation threshold in calculations, Ref. 7.
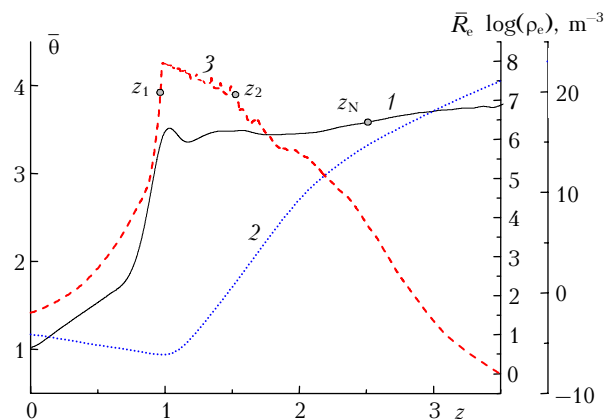

Fig. 7. Evolution along the optical path of the normalized global angular beam divergence $\bar{\theta} = \theta(z)/\theta_D$ (*1*), the effective radius $\bar{R}_e = R_e(z)/R_0$ (*2*), and peak number density of free electrons ρ_e (*3*) at propagation of a femtosecond pulse with $\eta = 2$. The points on curve *3* correspond to the conventional boundaries of light filament existence; z_1 is the filament onset (nonlinear beam focus); z_2 is its end; z_N is boundary of medium nonlinearity.

The decrease of the global beam divergence following the maximum of $\bar{\theta}(z)$ corresponds to the stage of filament stabilization when the plasma nonlinearity prevents further transverse beam compression and its size R_{-1} fluctuates about a some mean level ∼ 80 μm (see Fig. 1). The calculations

indicate that in this zone the spatial beam profile is of the form of a central peak surrounded by a system of concentric rings formed due to the interference of the beam field periphery and its central part at subsequent re-focusing of time sections of the pulse. The divergence of such a beam is higher than the initial one, and the mean value of the parameter $\bar{\theta}$ is about 3.5 (for the initial power $\eta = 2$). If we compare the absolute values of the global and spectral radiation divergences in this zone, we will see that the angular size of spectral components of supercontinuum may be several times higher than the beam divergence as a whole.

As the laser pulse propagates further through the medium, the modulation beam instability in the medium together with the dispersive spread and energy losses for plasma formation disturb the conditions of the field self-channeling near the axis, and the light filament extinguishes (point z_2 in Fig. 7).

Starting from this point the diffraction beam broadening prevails over Kerr focusing that results in gradual disappearance of rings in the transverse energy profile $w(\mathbf{r}_\perp)$, and its transformation to unimodal distribution and gradual increase of the parameter $\bar{\theta}$.

After the filament extinguishes gradual growth of the parameter $\bar{\theta}$ occurs towards the end of the path of propagation that approaches, after some distance z_N, (the length of the nonlinearity zone) to an asymptotic level that points to the termination of the radiation self-action in the medium and formation of the limiting beam divergence $\tilde{\theta}_\infty$.

Figure 7 also shows the dependence of an effective beam radius

$$R_e^2 = 1/E(z) \int\limits_{-\infty}^{\infty} dt' \int\int\limits_{-\infty}^{\infty} d^2\mathbf{r}_\perp I(\mathbf{r}_\perp, z; t') \big|(\mathbf{r}_\perp - \mathbf{r}_{gr})\big|^2,$$

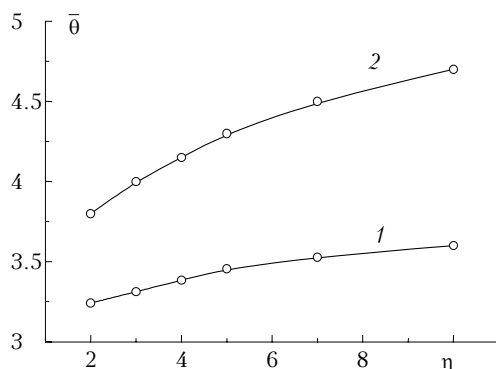on the normalized propagation distance, where r_{gr} is the radius-vector of the beam center of gravity.

Fig. 8. The normalized angular beam divergence $\bar{\theta}$ as a function of the initial power η. Dots present calculated data; solid lines are the spline-approximation; $z = 1$ (curve *1*) and $z = 4$ (curve *2*).

The increase of the initial power of a light beam also affects its global angular divergence $\bar{\theta}$. Thus, Figure 8 shows characteristic values of this parameter in two spatial zones, namely, in the zone where filamentation starts ($z = 1$) and in the path's end ($z = 4$). Within both segments presented the growth of global angular divergence $\bar{\theta}$ is observed with the increase of the radiation power that corresponds to the increase of the focal power of a nonlinear lens formed in the medium.

Conclusion

Thus, based on the unified parameters of a wave beam, we have numerically investigated the behavior of the frequency-angular spectrum and energy characteristics of the supercontinuum produced by a femtosecond light pulse propagated in the air. It has been found that the degree of nonlinear transformation of the frequency band of an ultrashort laser pulse caused by its nonstationary self-focusing is determined, after it passes the global nonlinear focus, by the length of the filamentation zone. In the extended filaments, a considerable transformation of energy of the initial radiation into the supercontinuum energy can take place, which is restricted only by nonlinear losses of radiation for plasma generation in the medium. The angular behavior of a femtosecond-duration light beam at self-action in the air is characterized by a sharp variation of its global divergence in the region of nonlinear focus, which is then changed by a smooth increase of the angular beam size in the filamentation zone and formation of the limiting divergence. This limiting divergence exceeds the initial one and increases with the growth of the radiation power. The angular size of the spectral components of the visible and infrared wings of supercontinuum radiation is higher than the beam divergence averaged over the spectrum as a whole.

Acknowledgments

References

1. V.P. Kandidov, O.G. Kosareva, E.I. Mozhaev, and M.P. Tamarov, Atmos. Oceanic Opt. **13**, No. 5, 394–401 (2000).
2. N. Aközbek, M. Scalora, C.M. Bowden, and S.L. Chin, Opt. Commun. **191**, Nos. 3–6, 353–362 (2001).
3. G. Mejean, J. Kasparian, J. Yu, S. Frey, E. Salmon, and J.-P. Wolf, Appl. Phys. B **78**, No. 5, 535–537 (2004).
4. Yu.E. Geints, A.A. Zemlyanov, G.M. Krekov, M.M. Krekova, and G.G. Matvienko, Atmos. Oceanic Opt. **19**, No. 10, 743–750 (2006).
5. A.A. Zemlyanov and Yu.E. Geints, Atmos. Oceanic Opt. **18**, No. 10, 778–782 (2005).
6. J. Kasparian, R. Sauerbrey, D. Mondelain, S. Niedermeier, J. Yu, J.-P. Wolf, J.-B. Andre, M. Franco,

A.A. Zemlyanov and Yu.E. Geints

Vol. 20, No. 1 / January 2007 / Atmos. Oceanic Opt. 39

B. Prade, S. Tzortzakis, A. Mysyrowicz, M. Rodriguez, H. Wille, and L. Wöste, Opt. Lett. **25**, No. 18, 1397−1399 (2000).

7. A.A. Zemlyanov and Yu.E. Geints, Atmos. Oceanic Opt. **18**, No. 7, 514−519 (2005).

8. A. Talebpour, S. Petit, and S.L. Chin, Opt. Commun. **171**, Nos. 4−6, 285−290 (1999).

9. E.T.J. Nibbering, G. Grillon, M.A. Franco, B.S. Prade, A. Mysyrowicz, J. Opt. Soc. Am. B **14**, No. 3, p. 650−655 (1997).

10. S.A. Akhmanov, V.A. Vysloukh, and A.S. Chirkin, *Optics of Femtosecond Pulses* (Nauka, Moscow, 1988), 312 pp.

11. E.T.J. Nibbering, P.F. Curley, G. Grillon, B.S. Prade, M.A. Franco, F. Salin, and A. Mysyrowicz, Opt. Lett. **21**, No. 1, 62−64 (1996).

12. V.P. Kandidov, O.G. Kosareva, A. Brodeur, C.J. Chien, and S.L. Chin, Opt. Lett. **22**, No. 17, 1332−1334 (1997).

13. I.S. Golubtsov, V.P. Kandidov, and O.G. Kosareva, Atmos. Oceanic Opt. **14**, No. 5, 303−315 (2001).

14. V.P. Kandidov, O.G. Kosareva, I.S. Golubtsov, W. Liu, A. Becker, N. Aközbek, C.M. Bowden, and S.I. Chin, Appl. Phys. B **77**, Nos. 2−3, 149−165 (2003).

15. P. Wasylczyk, W. Wasilewski, M. Trippenbach, and C. Radzewicz, Proc. SPIE **5949**, 321−325 (2005).

16. D. Faccio, P.D. Frapani, S. Minardi, A. Bramati, F. Bragheri, C. Liberale, V. Degiorgio, A. Dubietis and A. Matijosins, J. Opt. Soc. Am. B **22**, No. 4, 862−869 (2005).

17. V.E. Zuev, A.A. Zemlyanov, and Yu.D. Kopytin, *Nonlinear Atmospheric Optics* (Gidrometeoizdat, Leningrad, 1989), 256 pp.